inventions

MDPI

Article

Experimental Assessment of a Novel Dual Opening Dewar for Use on a Liquid Air Energy Storage System Installed on Remote, Islanded, Renewable Microgrids

Christofer Fackrell [1], Anthony Pollman [1,*], Douglas L. Van Bossuyt [1,*] and Anthony J. Gannon [2]

[1] Department of Systems Engineering, Naval Postgraduate School, Monterey, CA 93943, USA
[2] Department of Mechanical and Aerospace Engineering, Naval Postgraduate School, Monterey, CA 93943, USA
* Correspondence: agpollma@nps.edu (A.P.); douglas.vanbossuyt@nps.edu (D.L.V.B.)

Abstract: Islanded, renewable energy microgrids for use at remote operating facilities reduce logistical burdens associated with fossil fuel based electrical power sources and provide greater operational flexibility; however, energy generation can be intrinsically intermittent on renewable microgrids. This intermittent electrical generation can be mitigated with electrical energy storage. Liquid air energy storage (LAES) is one promising technology proposed to meet this energy storage issue due to its high energy density and lack of geographical constraints. Small-scale microgrids may not have enough excess capacity to store pressurized liquid air (LA), and instead may rely on unpressurized LA storage and their associated unpressurized power recovery systems. Using commercial off-the-shelf components, this article conducts a performance-based tradespace study for several dual opening, unpressurized Dewar designs for use with Stirling- or Peltier-based power recovery cycles. The dual opening Dewar design is found to be ineffective for the short-term LA storage times necessary for small-scale microgrid use, primarily due to excessive conductive thermal losses; however, the design may be useful as a LA receiver and immediate use energy storage medium for a connected Stirling generator. A proposed alternative solution using a self-pressurized Dewar for LA storage and transport for microgrid applications is presented for future work.

Keywords: Dewar; liquid air; liquid air energy storage; renewable microgrid; islanded microgrid; remote microgrid; Stirling generator; Stirling cryocooler; Peltier thermoelectric generator

check for updates

Citation: Fackrell, C.; Pollman, A.; Van Bossuyt, D.L.; Gannon, A.J. Experimental Assessment of a Novel Dual Opening Dewar for Use on a Liquid Air Energy Storage System Installed on Remote, Islanded, Renewable Microgrids. *Inventions* **2022**, *7*, 101. https://doi.org/10.3390/inventions7040101

Academic Editors: Emilio Ghiani and Paolo Attilio Pegoraro

Received: 22 September 2022
Accepted: 7 November 2022
Published: 9 November 2022

1. Introduction

Historically, electrical grid energy sources have primarily come from fossil fuel based regional power stations, with backup sources of electrical power at an installation or facility level also relying on fossil fuel based energy, most commonly taking the form of emergency diesel generators (EDGs) [1]. This energy distribution model does not work when a regional powergrid is unavaible, such as remote research stations. Over the last several years there has been an increased interest regarding remote, islanded, and renewable energy microgrids for use in remote locations, allowing for a reduction in logistics burdens associated with fossil fuel based electrical power sources [2,3]. The Department of Energy (DOE) defines a microgrid as, "a group of interconnected loads and distributed energy resources within clearly defined electrical boundaries that acts as a single controllable entity with respect to the [electrical] grid. A microgrid can connect and disconnect from the grid to enable it to operate in both grid-connected or islanded-mode" [4] (p. 84). This definition can be modified to define a remote, islanded microgrid as one that does not connect to a larger, regional power grid [5]. Furthermore, a remote, islanded, and renewable microgrid is one that supplies the majority of its electrical power from renewable sources, such as wind and solar [6]. While these type of microgrids aim to address electrical energy supply issues for isolated locations, the energy generated by them is intrinsically intermittent due to the microgrid's reliance on renewable energy sources, which are often cyclic in their energy

production (e.g., photovoltaic cells only producing electrical power at night) [7]. This can be mitigated with energy storage, which enables electrical power to be sent to islanded, renewable microgrids when their renewable energy sources are incapable of meeting the grid's electrical power demands [8].

Energy storage on microgrids during power interruption presents its own problems [9]. Typically, when a renewable energy power source supplies electrical power that is greater than the grid's electrical demand, the electrical supply is metered down, as is the case of wind turbines, or it is rejected as heat via a resister bank for non-adjustable sources such as photovoltaic cells; however, with attached microgrid energy storage this excess electrical power can be used to store energy for later use [10,11]. Several generalized types of energy storage systems exist, including electrical, mechanical, thermal, chemical, electrochemical, and magnetic; each of these solutions has their own set of advantages and disadvantages, including cost, size, energy density, efficiency, lifespan, charging rate, reliability, ease of use, environmental impact, life cycle cost, and disposability [1,12,13]. Additionally, depending on the storage method, the energy recovery options are limited, with each option having its own advantages and disadvantages [14]. This work focuses on thermal energy storage in the form of cryogenic liquid air (LA).

Typically, liquid air energy storage (LAES) systems are used for large or industrial-scale applications due to inefficiencies in liquifying air, which use one, or a combination of, several thermo-dynamic cycles, such as the Linde Hampson, Claude, mixed regrigerant, and Solvay cycles [15–17]. However, at smaller-scales, which would be viable on an islanded microgrid, these tradiational LAES systems use liquefaction and power-recovery cycles that are innapropriate due to excessive electrical power requirements for LA production andthe immense size of their componenets. Due to these electrical power and size considerations, other liquifaction options are considdered. This consideration at the microgrid level is made due to LA's high energy density and lack of geographic placement requirements like many similar renewable energy capture and storage techniques, such as compressed air energy storage (CAES) and pumped hydro [18,19]. The most common low-power liquifaction options, which are capable of being effectively power by an islanded microgrid, include the Stirling, pulse tube, Gifford-McMahon, Brayton, and Joule-Thomson cycles [17]. This combination of unfetted access to air, coupled with a high energy density, makes investigation into LAES for remote, islanded, renewable microgrids a useful endeaver.

Previous work on small-scale LAES has primarily focused on feasibility, modeling, or component performance analyses. Building on the work of Joshi and Patel, and Howe et al., Willis et al. modeled a small-scale liquid air energy storage and expansion system using a process modeling and simulation software common to the oil and gas industry [20–22]. Girouard et al. and Fredrickson et al. proposed component selection for a scaled-down version of an industrial LA energy storage process [23,24]. These investigations showed that turbine and other similar industrial level technologies do not scale well, and subsequent analyses focused on cycles and technologies that were more promising for small-scale applications, agreeing with work presented by Damak et al. [16,25–28]. Two of these promising small-scale energy recovery methods are a Stirling generator, using a Stirling cycle, and a thermoelectric generator, leveraging the Peltier effect [27,29]. The patent application for a dual Stirling cycle liquid air battery by Bailey et al. uses a wide mouth Dewar that contains a lower-power Stirling cryocooler for liquefaction and Stirling generator power recovery [27]. This combination of Stirling cycles provides a low-power method of producing LA at atmospheric pressure, while allowing for the recovery of electrical power from the LA at the same atmospheric pressure.

A Dewar is a vessel designed to store cryogenic fluids by minimizing heating of the stored fluid by conduction, convection, and radiative heat transfer, which causes evaporation of the LA, preventing its stored energy from being used for other applications [30]. In its simplest form, a Dewar has an inner and outer wall with a vacuum drawn between them to minimize thermal conductivity, a low emissivity reflective radiation shield to minimize radiative heating, and a lid or stopper at the mouth of the Dewar to minimize the vapor

mass flow rate of the stored liquid as it evaporates, thus limiting thermal convection [31]. Atmospherically vented storage Dewars typically use a long and narrow neck, as this lowers the overall heat flux conducted down the neck, reducing the LA evaporation rate [32,33]. Additionally, typical storage Dewars contain a spherical or semi-spherical storage area to maximize the volume of LA to the physical surface area of the Dewar's material in contact with the LA [33]. This reduces conductive losses of the LA. The wide mouth Dewar design used by Bailey et al., necessary to support a Stirling cryocooler and generator in a single opening, increases the convection energy losses compared to narrow neck Dewar variants and relies on an extended cold side of the Stirling generator to be in contact with LA throughout the storage volume, which also increases conduction due to its continuous contact with the stored LA [27].

This article explores alternatives to Bailey et al.'s Dewar design that may be efficacious in improving energy extraction from LA for small-scale LAES applications connected to a microgrid using a non-pressurized LA storage and energy recovery system. Specifically, it explores the use of a two opening Dewar, with the opening at the top designated for a cryocooler to produce LA and a second penetration of the Dewar at the bottom used for a power recovery cycle. This design reduces the width of the upper Dewar neck, reducing convection from the surface of the LA while also reducing the higher conductivity associated with a wider Dewar mouth. The lower port allows for energy extraction from the LA's entire stored volume as it evaporates without the need for an extended cold side for an attached Stirling generator. This configuration does increase the conductive losses of the Dewar, which is the performance-based tradespace that will be explored. Additionally, this Dewar configuration could be adapted to other low pressure energy recovery methods, such as a thermoelectric generator.

2. Materials and Methods

This research utilized commercial off-the-shelf (COTS) components and readily available additive manufactured apparatuses to explore the evaporative performance tradespace of a dual opening Dewar. This comparison was done by measuring the evaporation rate (g/min) of liquid nitrogen (LN2), which is readily commercially available, for each Dewar configuration and graphing the LN2 mass versus elapsed time.

To facilitate rapid, low-cost Dewar experimentation, 473 mL Hydroflask TempShield bottles were used, which were found to have a comparable physical design to typical experimental Dewars and have been shown to be efficacious in approximating their performance [31,34]. These bottles contain a 1 mm thick stainless-steel outer shell, a 0.75 mm thick stainless-steel inner shell, a vacuum jacket between these shells, and physical contact between the shells only occurring at the top mouth of the bottle. The baseline bottle was modified to create an additional five experimental Dewar configurations.

Each flask was placed on a 3D printed polylactic acid (PLA) plastic cylinder (3 in outside diameter, 2 in inside diameter, 2 in height, density 0.33 g/cm^3). The 2 in inner cavity of the plastic cylinder was filled with low-density polyurethan ether foam (density 0.03 g/cm^3) to provide support for experimental Dewar modifications. An additional polyurethan ether foam cylinder (62 mm diameter, 50 mm height) was used to cover the mouth of the experimental Dewars to limit convective heat transfer differences that might be caused by natural room air current fluctuations.

Data collection runs started with a temperature equalization step, which required filling the experimental Dewar with 350 g of LN2 and allowing 300 g of the LN2 to evaporate or 1 h to elapse, whichever came first. After temperature equalization, the experimental Dewar was again filled to a level of 350 g of LN2 and evaporation data was recorded and graphed between LN2 levels of 300 g to the first LN2 mass measurement of 50 g, or less, on its standard data recording cycle. The mass data recording cycle was once per minute for the modified experimental Dewars and once per 10 min for the baseline, unmodified experimental configuration. To measure the change in LN2 mass, two laboratory scales were used: an Ohaus CS 5000 and a Bonvoisin BCS-30. Four data runs for each experimental

configuration were conducted and then averaged together. The experimental results were graphed and normalized exponential decay evaporation equations were determined using MATLAB, which approximated the various complex heat transfer mechanism taking place [30]. Stagnant air within the experimental area was maintained to the greatest extent possible to limit airflow and changes in humidity and lighting conditions were maintained constant. Ambient temperature ranged from 20.1°C to 21.9°C. The basic experimental setup used for each data run is shown in Figure 1.

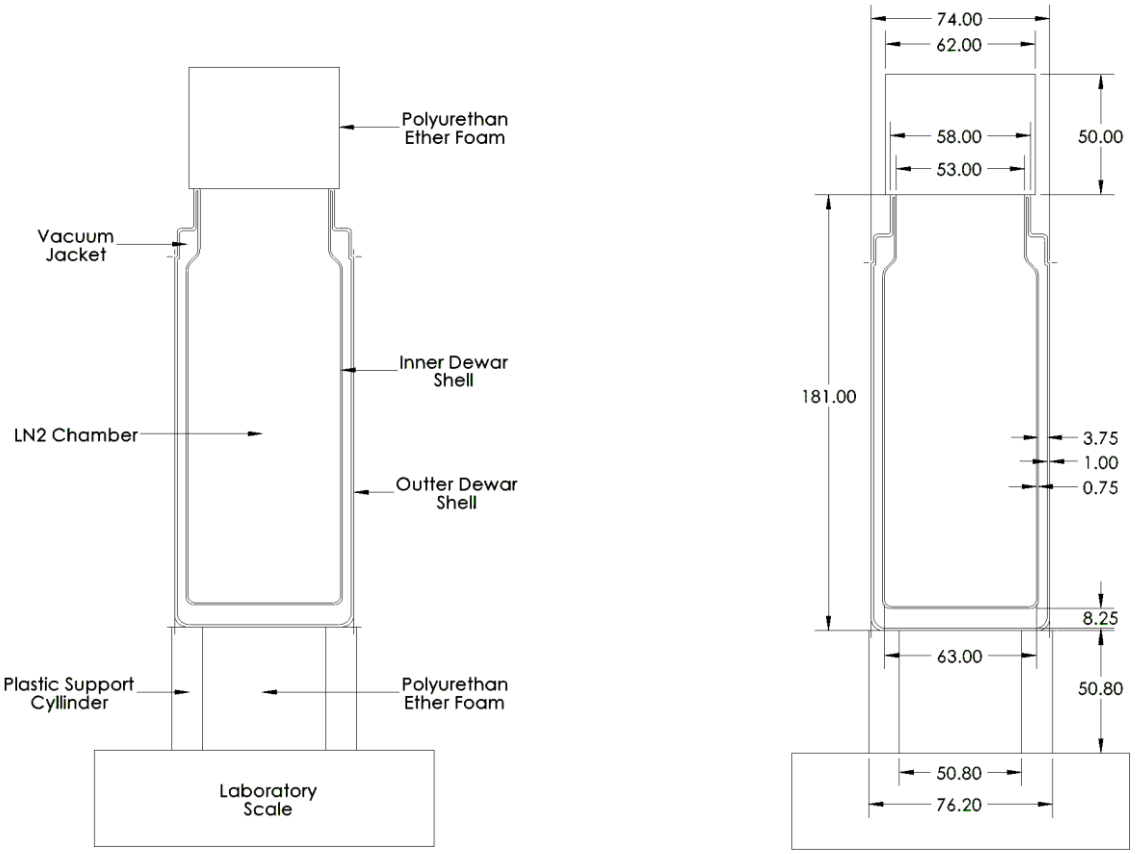

(**a**) (**b**)

Figure 1. (**a**) Basic experimental setup with component labels with baseline configuration shown; (**b**) Basic experimental setup characteristic dimensions with baseline configuration shown. All measurements are shown in mm.

Six different experimental Dewar configurations were analyzed for LN2 evaporation rates: a baseline, unmodified 473 mL Hydro Flask TempShield bottle; an experimental Dewar configuration that modifies the baseline by removing the vacuum jacket; an experimental Dewar configuration without a vacuum jacket containing a brass fitting at the bottom of the Dewar that does not come in physical contact with the outer Dewar shell; an experimental Dewar configuration without a vacuum jacket with a Teflon fitting at the bottom of the Dewar; an experimental Dewar configuration without a vacuum jacket and a brass fitting at the bottom of the Dewar; and an experimental Dewar with a vacuum jacket and a brass fitting at the bottom of the Dewar. The baseline Dewar configuration did not modify the physical structure of the bottle, while the five experimental Dewar configurations modified this baseline in some way.

The experimental Dewar without a vacuum jacket modified the baseline configuration by drilling a 5/32 in (4 mm) hole into the center-bottom of the baseline bottle's outer shell. The purpose of this test configuration was to measure the effect of the vacuum jacket on LN2 evaporation rate compared to the baseline.

The experimental Dewar without a vacuum jacket with a brass fitting at the bottom of the Dewar that does not come in physical contact with the outer Dewar shell was modified to assess the effect of conduction between the brass fitting and the outer Dewar shell. A 1-9/64 in (29 mm) hole was drilled in the center-bottom of the outer Dewar shell and a 1/4in NPT threaded tap was drilled into the center-bottom of the inner shell. A 1/4 in NPT, 1-1/2 in long, brass double end threaded fitting with a 1/4 in NPT cap on one side was threaded into the tap on the inner Dewar wall and sealed with cryogenic rated Scotch-Weld Epoxy Adhesive 2216 B/A Gray.

The experimental Dewar with a vacuum jacket and a brass fitting at the bottom of the Dewar was modified to support the bottom brass fitting and to restore the vacuum to the Dewar. A 1/4 in NPT threaded tap was drilled into the center-bottom of the Dewar's inner and outer shell. A 1/4in NPT, 1-1/2 in long, brass dual threaded fitting with a 1/4 in NPT cap was threaded into this tap and sealed with cryogenic rated Scotch-Weld Epoxy Adhesive 2216 B/A Gray. A 1/4 in NPT hole was drilled into the outer Dewar wall 90 mm from the base, allowing for a 1/4 in NPT brass vacuum ball valve to be installed with a 1/4in brass barbed hose fitting. This facilitated a 29.9 in Hg vacuum to be drawn between the inner and outer Dewar shells. Scotch-Weld Epoxy Adhesive 2216 B/A Gray was used to seal the vacuum ball valve to the outer Dewar wall. This configuration allowed for the assessment of LN2 evaporation rate due to the conductive effects through the installed brass fitting to the outer Dewar wall. This same experimental Dewar configuration was also used to determine the LN2 evaporation rate without a vacuum by maintaining the brass vacuum ball valve open.

The experimental Dewar without a vacuum jacket and a Teflon fitting at the bottom of the Dewar was modified in the same way as the Dewar with a vacuum jacket and a brass fitting, except a Teflon fitting of the same dimensions as the brass fitting was used; however, a constant vacuum could not be maintained using the Teflon fitting. This configuration enabled assessing the use of a Teflon, vice brass, fitting material on LN2 evaporation rate. This was done because Teflon has a lower heat transfer coefficient than brass, which was hypothesized to lower convective heat losses to the outer Dewar shell compared to an equivalent configuration using brass [35].

These six experimental configurations were assigned an experiment configuration designator, A through F, as described in Table 1.

Physical representations of the experimental Dewar configurations are shown in Figure 2. The scale, PLA support cylinder, and low-density polyurethan ether foam are not shown but are used the same as in Figure 1 during data collection runs. Specific Dewar measurements are not shown but are to scale to those provided in Figure 1.

Table 1. Experimental Dewar configuration designations for the baseline Hydro Flask and five modified configurations of the baseline.

Experimental Dewar Configuration	Description
A	Baseline 473 mL Hydro Flask TempShield bottle-Dewar with no modification. Contains a vacuum jacket.
B	Modified baseline bottle-Dewar with a hole in the bottom outer shell and no vacuum jacket.
C	Modified baseline bottle-Dewar with a hole in the bottom outer and inner shells, a bottom mounted capped brass fitting that does not have metal-metal conduction to the outer bottle-Dewar shell, and no vacuum jacket.
D	Modified baseline bottle-Dewar with a capped threaded Teflon fastener penetrating the bottom outer and inner shells with no vacuum jacket.
E	Modified baseline bottle-Dewar with a capped threaded brass fastener penetrating the bottom outer and inner shells with no vacuum jacket.
F	Modified baseline bottle-Dewar with a capped threaded brass fastener penetrating the bottom outer and inner shells with a vacuum jacket.

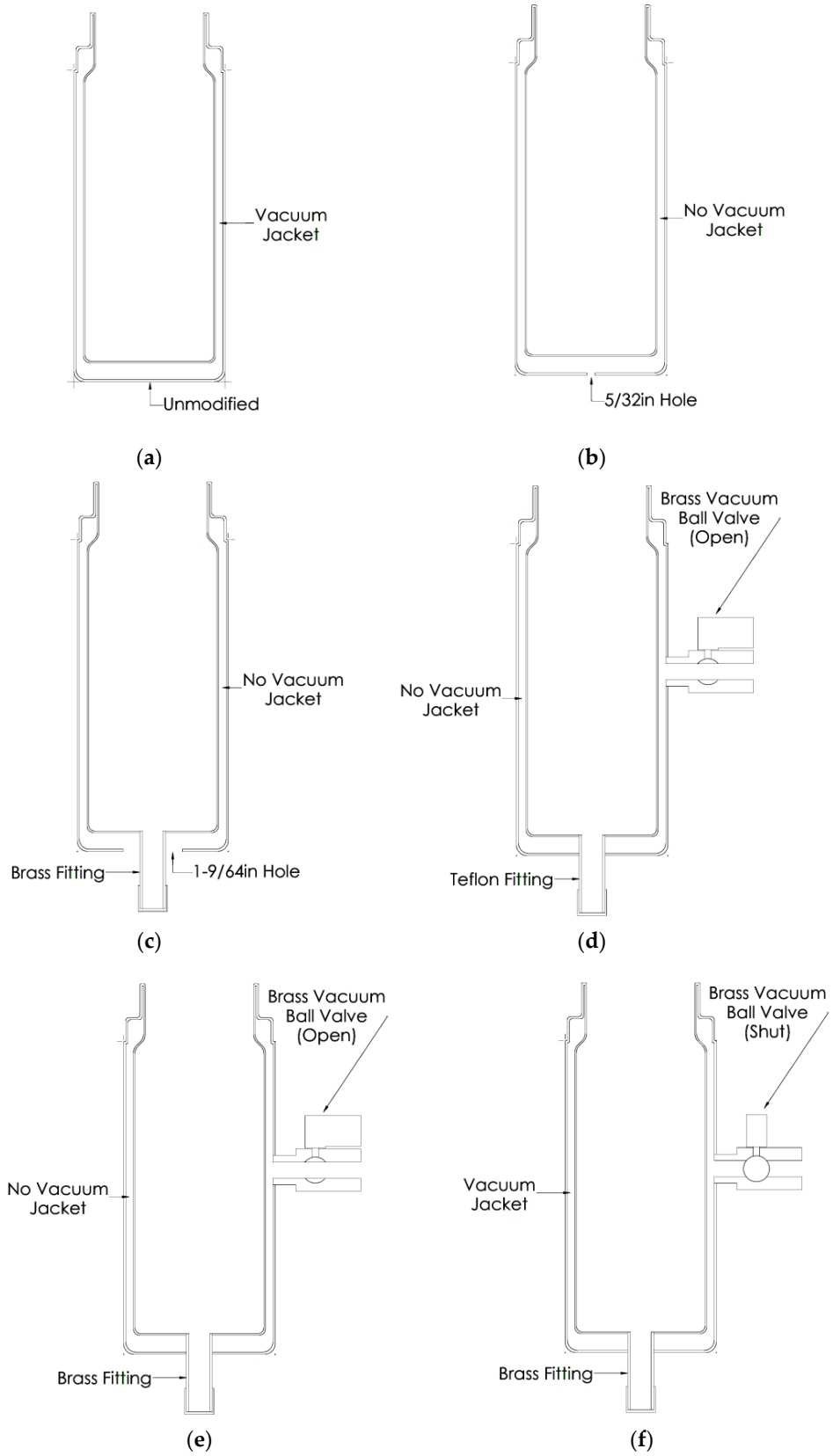

Figure 2. (**a**) Experimental configuration A; (**b**) Experimental configuration B; (**c**) Experimental configuration C; (**d**) Experimental configuration D; (**e**) Experimental configuration E; (**f**) Experimental configuration F. A 1/4 in brass barbed hose fitting was attached to the vacuum ball value for experimental configurations D, E, and F, but are not shown in this figure.

3. Results

Each experimental Dewar had four data runs collected. The average results of these runs for configurations B through F are shown in Figure 3. Raw data is provided in Appendix A.

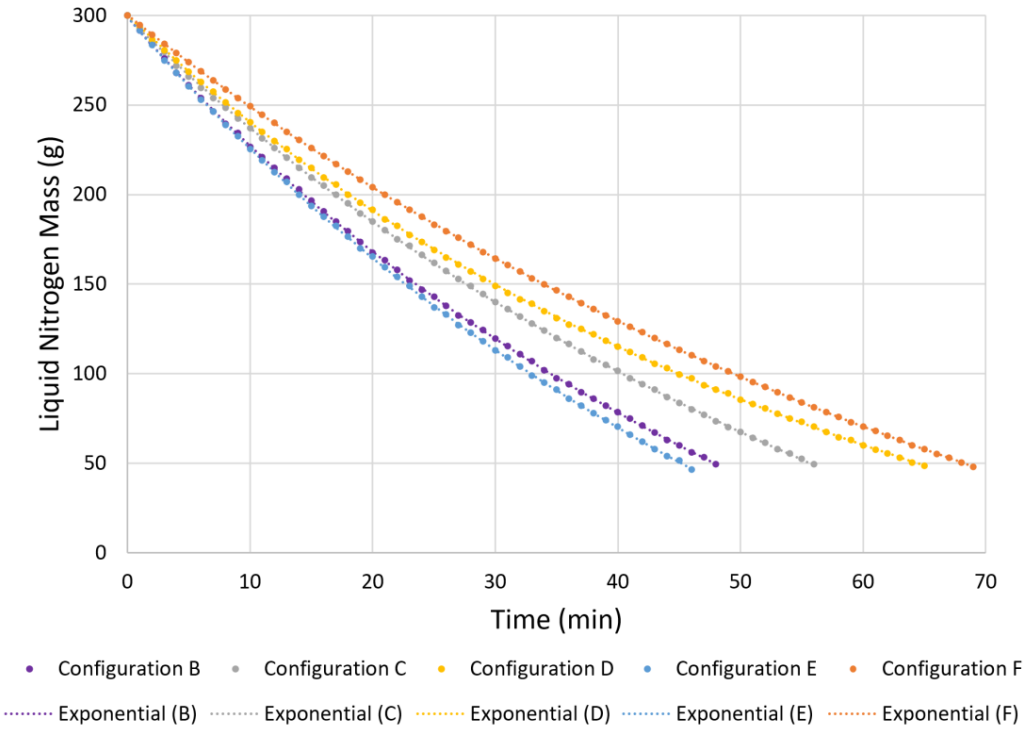

Figure 3. Evaporation rates for modified experimental Dewar configurations B, C, D, E, and F. Each curve is the average of four data runs, with data plotted in one-minute increments. Each data point's associated y-axis standard deviation (SD) is contained in Appendix A. All curves start at 300 g of LN2 and continue until the first averaged data point is less than or equal to 50 g of LN2.

The performance of each experimental Dewar is based on the Dewar's rate of LN2 evaporation, with higher evaporation rates being considered worse performance and lower evaporation rates being considered better. Experimental Dewar configuration F had the lowest evaporation rate among the modified Dewars, evaporating from 300 g of LN2 to 48 g of LN2 in 69 min. Aside from the baseline experimental Dewar configuration A, presented in Figure 4, which evaporates from 300 g to 49 g of LN2 in 570 min, configuration F was the only Dewar configuration which contained a vacuum jacket. This highlights the importance of a vacuum jacket with regard to Dewar performance. Despite this enhanced performance compared to the other modified Dewar configurations, the holding time of LN2 for Dewar configuration F is only 12.1% of the baseline Dewar, configuration A. This is due to conduction directly to the outer Dewar shell via the brass fitting, which in turn increases the convective heat transfer to the atmospheric air in contact with the outer Dewar shell.

The worst performing experimental Dewar was configuration E, which had 253.5 g of LN2 evaporate in 46 min. The difference between this configuration and configuration F was that the vacuum port for configuration E was opened to remove the vacuum jacket. The removal of the vacuum allowed air to be in the vacuum space, dramatically increasing the convection taking place between the inner Dewar shell to the outer Dewar shell. Additionally, gaseous airflow can occur at the opening of the vacuum ball valve, meaning an increase in convective heat transfer occurs as warm air is permitted to more freely flow into the gap between the Dewar shells. This performance drop between the best and worst performing configurations once again emphasizes the importance of a vacuum

jacket between Dewar shells to reduce thermal convective and conductive losses, as the physical design was exactly the same and only the presence of a vacuum differentiated these two configurations.

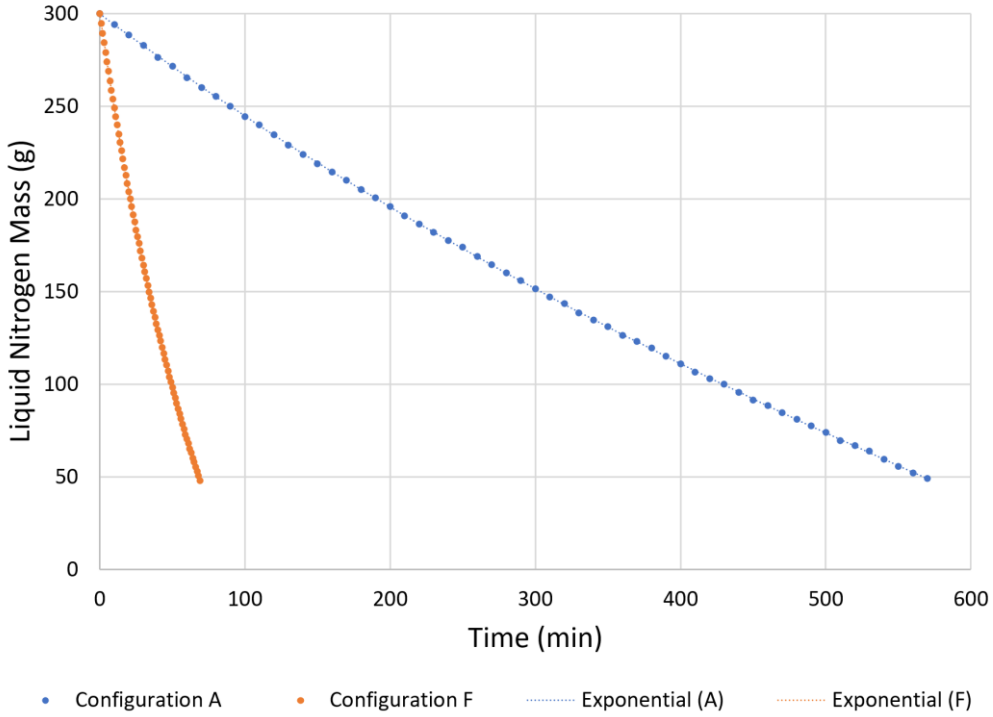

Figure 4. Evaporation rate of the baseline Dewar, configuration A, and the highest performing modified experimental Dewar, configuration F. Each curve is the average of four data runs, with data plotted in ten-minute increments for configuration A and one-minute increments for configuration F. Each data point's associated y-axis SD is contained in Appendix A. Both curves start at 300 g of LN2 and continue until the first averaged data point is less than or equal to 50 g of LN2.

The second best performing experimental Dewar was configuration D, which saw 251.5 g of LN2 evaporate in 65 min. Two differences existed between this configuration and configuration F. First, no vacuum jacket existed, with air being permitted to freely flow into and out of the vacuum ball valve, increasing the convective and conductive losses in the same way as discussed concerning Configuration E. Second, the brass fitting at the bottom of the experimental Dewar was replaced with a Teflon one of the same dimensions. Compared to the worst performing Dewar, configuration E, the only difference between them was this fitting material at the bottom of the Dewar. The combination of this information confirms that replacing the high thermal conductivity brass fitting with a lower conductivity material improves performance of a dual opening Dewar design by reducing conductive losses to the outer Dewar shell. The evaporation curve for configuration D (Figure 3) is also revealing. Compared to configurations B, C, E, and F, the slope of the curve levels out faster as the volume of LN2 decreases. This is likely caused by an increasing amount of conductive surface area in contact with the LN2 being Teflon as the LN2 level lowers, versus being the stainless-steel or brass that is present in the other modified experimental Dewar configurations. It is assumed that if configuration D was manufactured to hold a vacuum, such as configuration F, then the combination of a Teflon fitting and a vacuum jacket would prove to have better performance than configuration F.

Configuration C had the third best performance, with LN2 evaporating from 300 g to 49.5 g in 56 min. This configuration removed metal-to-metal conduction between the brass fitting and stainless-steel outer Dewar shell by removing a stainless-steel ring around the brass fitting. Though this configuration sacrifices being able to restore a vacuum to the Dewar, it still had better performance than Dewar configuration E; thus, it is confirmed that

the metal-to-metal conduction at the brass fitting interface is greater than the conduction of the brass-air-stainless steel interface produced. Despite this finding, it is still more advantageous to restore a vacuum jacket to the Dewar.

Experimental Dewar configuration B had the second worst performance, evaporating 250.5 g of LN2 in 48 min. This configuration merely removed the vacuum from between the inner and outer Dewar shells and did not add any brass fittings. Dewar configuration E had a similarly sized hole via the vacuum ball valve and barbed hose fitting, but also had the brass fitting protrude from the outer Dewar shell. The lack of this protrusion for configuration B likely accounts for its slightly better performance than configuration E.

Normalized exponential decay evaporation curve fit equations for each of the experimental Dewar Configurations were found using Equation (1).

$$y = (a)e^{-bx} + (c)e^{-dx} \quad (1)$$

where y is the normalized mass of LN2, x is the normalized elapsed experimental evaporation time, and a, b, c, and d are coefficients. Normalization was based on a 300 g LN2 initial mass and the associated evaporation time for a given experimental Dewar configuration. Table 2 contains the normalized evaporation equations and their associated R^2 value, as well as the final LN2 mass and evaporation time for each experimental Dewar configuration.

Table 2. Experimental Dewar LN2 normalized evaporation equations, R^2 values, final mass, and evaporation times. Initial LN2 mass for all configurations was 300 g with a start time of zero minutes. Evaporation equations are valid when both x and y values are positive.

Experimental Dewar Configuration	Normalized Evaporation Equation and R^2 Value	Final LN2 Mass (g)	Evaporation Time (min)
A	$y = 1.147e^{-0.8685x} - 0.1477e^{0.7679x}$ $R^2 = 1.0000$	49.0	570
B	$y = 1.081e^{-1.121x} - 0.08338e^{0.811x}$ $R^2 = 1.0000$	49.5	48
C	$y = 1.102e^{-1.07x} - 0.1056e^{0.7096x}$ $R^2 = 1.0000$	49.5	56
D	$y = 1.045e^{-1.317x} - 0.04467e^{0.967x}$ $R^2 = 1.0000$	48.5	65
E	$y = 1.207e^{-0.9559x} - 0.2102e^{0.3818x}$ $R^2 = 1.0000$	46.5	46
F	$y = 1.231e^{-0.9628x} - 0.2302e^{0.2965x}$ $R^2 = 1.0000$	48.0	69

4. Discussion

The LN2 storage performance of experimental Dewar configuration F is only 12.1% that of the baseline Dewar, configuration A. Despite the vacuum jacket greatly minimizing conduction through the vacuum space between the inner and outer Dewar shells, the increase in conduction between the bottom fittings and the outer Dewar shell, as well as the air and insulating foam around the producing fitting, greatly reduces the efficacy of LN2 storage, making the configuration F inappropriate for a system designed to produce LA in the container for later use on a small-scale remote, islanded, renewable microgrid. This is because these microgrids typically require the use of their stored within a day after production, such as during the night for solar power-based microgrids. Despite this,

configuration F could be useful as a LA receiving vessel for a Stirling generator connected to the bottom port. This is because the energy lost at the bottom port is primarily conductive in nature and could be converted into electrical energy through an attached Stirling generator, with further energy recovery improvements possible by combining the Stirling generator with low temperature optimized thermoelectric generators (TEGs) on the outer Dewar shell. Additional cost–benefit analysis should be conducted as future work to determine which experimental Dewar configuration provides the most favorable solution, if this dual opening Dewar design is pursued for use as this immediate LA storage device.

The performance improvement gained by using a Teflon fitting in Configuration D, compared to the brass fitting used in configuration E, provides sufficient evidence that replacing additional metallic Dewar material with Teflon may prove to further improve the dual opening Dewar design. If manufacturing of this Teflon based Dewar can also support a vacuum jacket, then performance should exceed that of configuration F, the best performing modified Dewar. This investigation is the basis for the patented Dewar design mentioned in Section 6.

Overall, these findings show that the dual opening Dewar design is insufficient for efficacious storage of LA for a directly connected cryocooler and energy recovery cycle. An alternative design is next proposed for development as future work. The proposed future design uses a COTS storage Dewar with a cryocooler connected to the top of the Dewar's neck. An elongated displacer chamber, or equivalent, would extend the cold finger of the cryocooler below the bottom of the neck and into the main storage volume of the Dewar, allowing for effective production of LA. It is proposed that the cryocooler make a pressure-tight connection with the Dewar upper opening except for two ports for connected tubing. One of these ports requires connection to a short tube to act as an air vent of the Dewar, allow for air to enter the Dewar for liquification during cryocooler operation and to prevent overpressure during normal LA storage. This vent would have a normally open electrical solenoid valve attached to it such that when the valve is energized and shuts the upper portion of the Dewar can be pressurized. Normal evaporation of LA in the Dewar would naturally increase its pressure. As pressure increases it forces the LA to travel through a low thermal conductivity tube, such as Teflon, that travels from the bottom of the LA storage volume and passes through the second port at the Dewar neck to a power recovery phase. This tube would act as a smaller, secondary neck of the Dewar, meaning it would slightly increase conductive losses via the neck opening, though this is likely minimal. Once a sufficient volume of LA has been delivered to the power recovery component, the solenoid valve would deenergize, reliving the internal pressure of the Dewar and allowing the LA to continue long-term, efficient storage. Figure 5 outlines a physical configuration for this proposed system.

This proposed LA storage Dewar configuration takes advantage of modern, optimized unpressurized Dewar design elements, which will allow for longer LA storage times while also leveraging natural evaporative processes to facilitate the resultant pressure increase to transport LA from storage to a power recovery cycle. This design does add a small, periodic electrical load via the solenoid valve compared to a design that must only intermittently operate a cryocooler. Since both the cryocooler and solenoid valve must be operated with any microgrid configuration integrating this LAES system, a control system for them must be in place. This control system would likely be able to integrate with the control logic that already exists for the microgrid, but the additional electrical load they draw must be accounted for in determining the net electrical power that would be recoverable by this design. It is recommended that a LA storage system following this design is built and tested for use on a small-scale remote, islanded, and renewable microgrid.

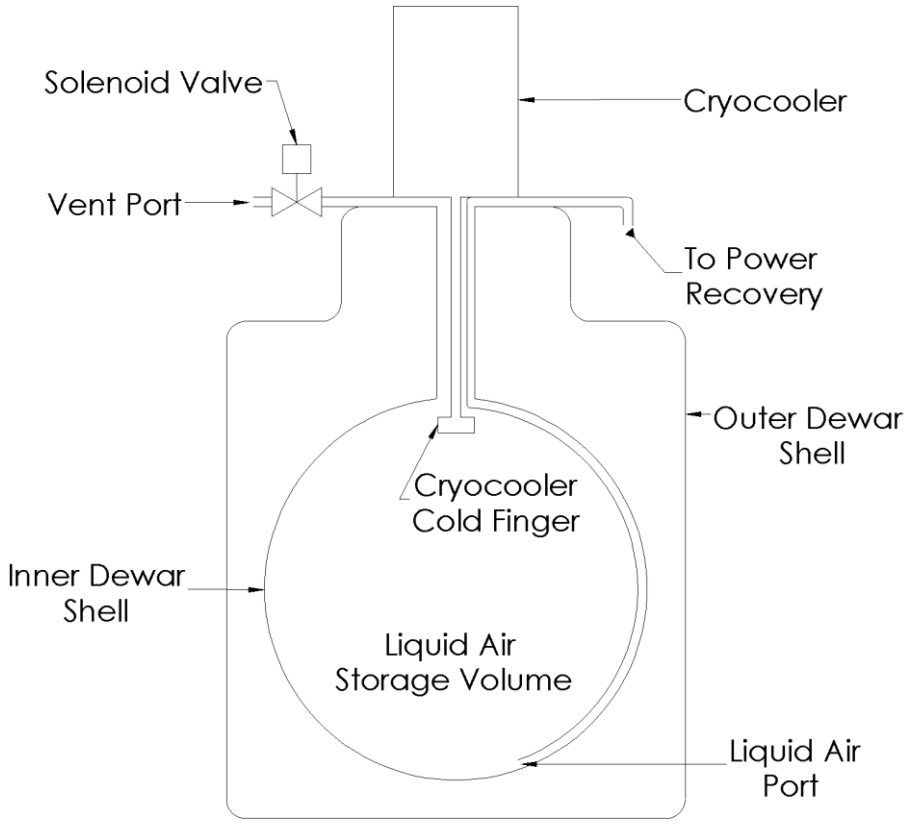

Figure 5. Proposed LA storage Dewar. The storage Dewar is normally unpressurized, but when power recovery is required by a connected microgrid, a solenoid valve on the vent port closes, allowing for a natural pressure increase to occur, forcing stored LA to be transported to a power recovery cycle.

5. Conclusions

A dual opening LA storage Dewar is not effective for storage times (i.e., 24 h) required for a small-scale remote, islanded, renewable microgrid due to excessive conductive thermal losses to the outer Dewar shell from the bottom opening. however, this dual opening Dewar design would be effective for the shorter-term LA holding required by processes that take advantage of immediate thermal energy conversion to electrical energy. These processes include a connected Stirling generator, a TEG, or a combination of these electrical energy production devices that take advantage of the thermal losses at the bottom opening. Further investigation may result in other uses for this system, such as controlled cooling of components. Additionally, the replacement of metallic portions of the dual opening Dewar with lower thermal conductivity material, such as Teflon, coupled with a vacuum jacket should be explored to further improve the performance of this dual opening design.

Due to the dual opening Dewar not being adequate for use in a LAES system using a normally unpressurized LA storage system, an alternative system should be perused. It is recommended that a COTS Dewar is developed and tested that is modified to allow for self-pressurization to low-pressures, allowing for LA transport from this high performance COTS Dewar to a separate power recovery subsystem that is not in continuous contact with the stored LA medium. This power recovery subsystem could utilize the vacuum jacketed dual opening Dewar design (i.e., Configuration F) presented in this work for immediate electrical power recovery from the LA via a connected Stirling generator, TEG, or combination of these devices.

6. Patents

Insights gained from the experimental Dewar configurations presented in Figure 3 resulted in the submission of US Patent Application 63/343,020, 2022, titled "Two Opening Dewar with Desiccant Annulus". This Dewar is designed to be the receiving vessel for LA being used in conjunction with a Stirling generator. The Dewar design leverages a vacuum jacket to reduce convective and conductive thermal losses; Teflon inner Dewar walls to reduce conduction; dual layer reflective shielding to minimize radiative losses; Teflon to metal interfacing at the bottom Dewar penetration to reduce conductive energy losses from the Stirling generator metal fitting to the outer Dewar wall; and has an integrated desiccant annulus to minimize long-term moisture and accumulation within the Dewar.

Author Contributions: Conceptualization, C.F. and A.P.; methodology, C.F. and A.P.; software, C.F. and A.P. validation, C.F., A.P. and A.J.G.; formal analysis, C.F.; investigation, C.F.; resources A.P.; data curation, C.F.; writing—original draft preparation, C.F.; writing—review and editing, C.F., D.L.V.B., A.J.G. and A.P.; visualization, C.F.; supervision, A.P., D.L.V.B. and A.J.G.; project administration, A.P. and D.L.V.B.; funding acquisition, A.P. All authors have read and agreed to the published version of the manuscript.

Funding: This research was funded by the NextSTEP Program through funding by the Office of Naval Research (ONR).

Data Availability Statement: The data presented in this study are included in Appendix A. Please contact the authors for additional questions concerning data analysis and interpretation.

Acknowledgments: Any opinions or findings of this work are the responsibility of the authors, and do not necessarily reflect the views of the U.S. Department of Defense or any other organizations. Approved for public release; distribution is unlimited.

Conflicts of Interest: The authors declare no conflict of interest.

Appendix A

Tables A1–A6 contain the raw mass data for each of the four data runs conducted for each experimental configuration, as well as average mass and the associated SD.

Table A1. Configuration A mass data.

Time (min)	Run 1 Mass (g)	Run 2 Mass (g)	Run 3 Mass (g)	Run 4 Mass (g)	Average Mass (g)	SD (g)
0	300	300	300	300	300.0	0.0
10	294	294	294	294	294.0	0.0
20	290	288	288	288	288.5	1.0
30	282	282	284	284	283.0	1.2
40	276	276	278	276	276.5	1.0
50	270	272	272	272	271.5	1.0
60	264	266	266	266	265.5	1.0
70	260	260	260	260	260.0	0.0
80	254	256	256	256	255.5	1.0
90	248	250	250	252	250.0	1.6
100	244	244	244	246	244.5	1.0
110	238	240	240	242	240.0	1.6
120	234	234	234	236	234.5	1.0
130	228	228	230	230	229.0	1.2
140	222	224	224	226	224.0	1.6
150	218	218	218	222	219.0	2.0
160	214	214	214	216	214.5	1.0
170	208	210	210	212	210.0	1.6
180	202	206	204	208	205.0	2.6
190	200	200	200	202	200.5	1.0
200	194	196	196	198	196.0	1.6
210	190	190	190	194	191.0	2.0

Table A1. *Cont.*

Time (min)	Run 1 Mass (g)	Run 2 Mass (g)	Run 3 Mass (g)	Run 4 Mass (g)	Average Mass (g)	SD (g)
220	186	186	186	188	186.5	1.0
230	180	182	182	184	182.0	1.6
240	176	178	176	180	177.5	1.9
250	172	174	174	176	174.0	1.6
260	168	170	168	170	169.0	1.2
270	164	164	164	166	164.5	1.0
280	158	160	160	162	160.0	1.6
290	154	156	156	158	156.0	1.6
300	150	152	152	152	151.5	1.0
310	146	148	146	148	147.0	1.2
320	142	144	144	144	143.5	1.0
330	138	138	138	140	138.5	1.0
340	132	136	134	136	134.5	1.9
350	130	130	132	132	131.0	1.2
360	124	128	126	128	126.5	1.9
370	120	124	124	124	123.0	2.0
380	118	120	120	120	119.5	1.0
390	112	116	116	116	115.0	2.0
400	110	110	112	112	111.0	1.2
410	104	108	106	108	106.5	1.9
420	100	104	104	104	103.0	2.0
430	98	100	100	102	100.0	1.6
440	94	96	96	96	95.5	1.0
450	90	92	92	92	91.5	1.0
460	86	88	90	90	88.5	1.9
470	84	84	84	86	84.5	1.0
480	80	80	82	82	81.0	1.2
490	76	78	78	78	77.5	1.0
500	72	74	74	76	74.0	1.6
510	68	68	70	72	69.5	1.9
520	66	66	68	68	67.0	1.2
530	62	64	64	66	64.0	1.6
540	58	60	60	60	59.5	1.0
550	54	56	56	56	55.5	1.0
560	50	52	52	54	52.0	1.6
570	48	50	48	50	49.0	1.2

Table A2. Configuration B mass data.

Time (min)	Run 1 Mass (g)	Run 2 Mass (g)	Run 3 Mass (g)	Run 4 Mass (g)	Average Mass (g)	SD (g)
0	300	300	300	300	300.0	0.0
1	290	292	292	292	291.5	1.0
2	284	284	284	284	284.0	0.0
3	276	276	274	278	276.0	1.6
4	268	268	266	270	268.0	1.6
5	262	260	260	262	261.0	1.2
6	256	254	252	254	254.0	1.6
7	248	246	244	248	246.5	1.9
8	240	240	238	240	239.5	1.0
9	236	234	232	236	234.5	1.9
10	228	226	224	228	226.5	1.9
11	222	220	220	222	221.0	1.2
12	216	214	214	216	215.0	1.2
13	210	208	208	210	209.0	1.2
14	204	202	202	204	203.0	1.2

Table A2. *Cont.*

Time (min)	Run 1 Mass (g)	Run 2 Mass (g)	Run 3 Mass (g)	Run 4 Mass (g)	Average Mass (g)	SD (g)
15	198	196	194	198	196.5	1.9
16	192	190	188	192	190.5	1.9
17	186	184	182	188	185.0	2.6
18	180	178	178	182	179.5	1.9
19	174	172	172	176	173.5	1.9
20	168	166	166	170	167.5	1.9
21	164	162	162	166	163.5	1.9
22	158	156	158	160	158.0	1.6
23	152	150	152	154	152.0	1.6
24	148	146	146	148	147.0	1.2
25	144	142	142	144	143.0	1.2
26	138	136	138	140	138.0	1.6
27	132	132	132	134	132.5	1.0
28	128	128	128	130	128.5	1.0
29	124	124	124	126	124.5	1.0
30	118	118	120	122	119.5	1.9
31	114	114	116	118	115.5	1.9
32	110	110	112	112	111.0	1.2
33	106	106	108	108	107.0	1.2
34	102	100	102	104	102.0	1.6
35	96	98	98	98	97.5	1.0
36	92	94	94	96	94.0	1.6
37	88	90	90	90	89.5	1.0
38	84	86	88	86	86.0	1.6
39	80	82	82	84	82.0	1.6
40	76	78	80	80	78.5	1.9
41	72	76	76	76	75.0	2.0
42	68	72	72	72	71.0	2.0
43	64	68	68	68	67.0	2.0
44	60	64	64	64	63.0	2.0
45	58	60	60	62	60.0	1.6
46	54	56	56	58	56.0	1.6
47	50	54	54	56	53.5	2.5
48	46	50	50	52	49.5	2.5

Table A3. Configuration C mass data.

Time (min)	Run 1 Mass (g)	Run 2 Mass (g)	Run 3 Mass (g)	Run 4 Mass (g)	Average Mass (g)	SD (g)
0	300	300	300	300	300.0	0.0
1	294	294	294	292	293.5	1.0
2	286	288	286	284	286.0	1.6
3	280	282	280	276	279.5	2.5
4	274	274	272	268	272.0	2.8
5	266	270	266	262	266.0	3.3
6	260	262	260	256	259.5	2.5
7	254	256	256	250	254.0	2.8
8	248	250	250	246	248.5	1.9
9	242	244	244	240	242.5	1.9
10	236	240	238	234	237.0	2.6
11	232	234	232	228	231.5	2.5
12	226	228	226	224	226.0	1.6
13	220	222	222	218	220.5	1.9
14	214	216	216	214	215.0	1.2
15	208	210	212	208	209.5	1.9
16	204	206	206	204	205.0	1.2

Table A3. *Cont.*

Time (min)	Run 1 Mass (g)	Run 2 Mass (g)	Run 3 Mass (g)	Run 4 Mass (g)	Average Mass (g)	SD (g)
17	198	200	202	200	200.0	1.6
18	194	194	196	196	195.0	1.2
19	188	190	190	190	189.5	1.0
20	184	184	186	186	185.0	1.2
21	180	180	180	180	180.0	0.0
22	174	174	176	176	175.0	1.2
23	170	170	174	172	171.5	1.9
24	166	164	168	168	166.5	1.9
25	160	160	164	164	162.0	2.3
26	156	156	158	160	157.5	1.9
27	152	150	154	156	153.0	2.6
28	148	148	148	152	149.0	2.0
29	144	142	146	146	144.5	1.9
30	138	138	142	142	140.0	2.3
31	134	134	138	138	136.0	2.3
32	132	130	132	134	132.0	1.6
33	126	126	130	130	128.0	2.3
34	122	122	126	126	124.0	2.3
35	118	118	122	122	120.0	2.3
36	116	114	118	118	116.5	1.9
37	112	110	114	114	112.5	1.9
38	106	106	110	110	108.0	2.3
39	104	102	106	108	105.0	2.6
40	100	100	102	104	101.5	1.9
41	96	96	98	100	97.5	1.9
42	92	92	96	96	94.0	2.3
43	90	88	92	94	91.0	2.6
44	86	84	90	88	87.0	2.6
45	82	82	84	86	83.5	1.9
46	78	78	82	82	80.0	2.3
47	76	74	78	80	77.0	2.6
48	72	72	74	76	73.5	1.9
49	70	68	70	72	70.0	1.6
50	66	66	68	70	67.5	1.9
51	62	62	66	66	64.0	2.3
52	60	60	62	64	61.5	1.9
53	56	56	60	60	58.0	2.3
54	54	54	56	58	55.5	1.9
55	50	52	54	54	52.5	1.9
56	48	48	50	52	49.5	1.9

Table A4. Configuration D mass data.

Time (min)	Run 1 Mass (g)	Run 2 Mass (g)	Run 3 Mass (g)	Run 4 Mass (g)	Average Mass (g)	SD (g)
0	300	300	300	300	300.0	0.0
1	292	292	294	294	293.0	1.2
2	286	286	288	286	286.5	1.0
3	282	280	280	280	280.5	1.0
4	276	274	276	274	275.0	1.2
5	270	268	268	268	268.5	1.0
6	264	262	264	262	263.0	1.2
7	258	258	258	256	257.5	1.0
8	252	252	252	250	251.5	1.0
9	246	246	246	244	245.5	1.0
10	240	242	240	240	240.5	1.0

Table A4. *Cont.*

Time (min)	Run 1 Mass (g)	Run 2 Mass (g)	Run 3 Mass (g)	Run 4 Mass (g)	Average Mass (g)	SD (g)
11	234	236	236	234	235.0	1.2
12	230	232	230	228	230.0	1.6
13	226	226	226	224	225.5	1.0
14	220	220	220	218	219.5	1.0
15	214	216	216	214	215.0	1.2
16	210	210	210	208	209.5	1.0
17	206	206	206	204	205.5	1.0
18	200	200	200	200	200.0	0.0
19	196	196	196	194	195.5	1.0
20	192	192	192	190	191.5	1.0
21	186	186	186	186	186.0	0.0
22	182	184	182	182	182.5	1.0
23	178	178	178	176	177.5	1.0
24	172	174	176	172	173.5	1.9
25	168	170	170	168	169.0	1.2
26	164	166	166	164	165.0	1.2
27	160	162	162	160	161.0	1.2
28	156	158	158	156	157.0	1.2
29	152	154	154	152	153.0	1.2
30	148	150	150	148	149.0	1.2
31	144	146	146	144	145.0	1.2
32	142	142	142	140	141.5	1.0
33	138	140	140	138	139.0	1.2
34	134	136	136	134	135.0	1.2
35	130	132	132	130	131.0	1.2
36	128	128	128	126	127.5	1.0
37	124	126	126	124	125.0	1.2
38	122	122	124	120	122.0	1.6
39	118	120	120	116	118.5	1.9
40	114	116	116	114	115.0	1.2
41	112	114	112	110	112.0	1.6
42	108	110	110	108	109.0	1.2
43	106	106	106	104	105.5	1.0
44	102	104	104	102	103.0	1.2
45	100	100	100	98	99.5	1.0
46	98	98	98	96	97.5	1.0
47	94	94	94	92	93.5	1.0
48	90	92	92	90	91.0	1.2
49	88	90	90	88	89.0	1.2
50	86	86	86	84	85.5	1.0
51	82	84	84	82	83.0	1.2
52	80	80	82	80	80.5	1.0
53	78	78	78	76	77.5	1.0
54	74	76	76	74	75.0	1.2
55	72	74	74	72	73.0	1.2
56	70	72	72	68	70.5	1.9
57	66	68	70	66	67.5	1.9
58	64	66	66	62	64.5	1.9
59	64	64	64	60	63.0	2.0
60	60	60	62	58	60.0	1.6
61	58	58	58	56	57.5	1.0
62	56	56	56	54	55.5	1.0
63	52	54	54	52	53.0	1.2
64	50	52	52	48	50.5	1.9
65	48	50	48	48	48.5	1.0

Table A5. Configuration E mass data.

Time (min)	Run 1 Mass (g)	Run 2 Mass (g)	Run 3 Mass (g)	Run 4 Mass (g)	Average Mass (g)	SD (g)
0	300	300	300	300	300.0	0.0
1	292	290	292	292	291.5	1.0
2	284	282	284	284	283.5	1.0
3	276	274	276	274	275.0	1.2
4	270	266	270	266	268.0	2.3
5	262	258	262	260	260.5	1.9
6	254	252	254	252	253.0	1.2
7	248	244	248	246	246.5	1.9
8	240	238	240	238	239.0	1.2
9	234	230	234	232	232.5	1.9
10	228	224	226	224	225.5	1.9
11	220	218	220	218	219.0	1.2
12	214	210	214	212	212.5	1.9
13	208	206	208	206	207.0	1.2
14	200	200	200	200	200.0	0.0
15	194	192	194	194	193.5	1.0
16	188	186	188	188	187.5	1.0
17	184	180	184	182	182.5	1.9
18	178	174	178	176	176.5	1.9
19	170	168	172	170	170.0	1.6
20	166	164	166	166	165.5	1.0
21	160	158	160	160	159.5	1.0
22	154	152	156	154	154.0	1.6
23	150	146	150	150	149.0	2.0
24	144	140	144	144	143.0	2.0
25	138	134	138	138	137.0	2.0
26	134	130	134	134	133.0	2.0
27	128	124	128	128	127.0	2.0
28	124	120	124	124	123.0	2.0
29	118	116	120	118	118.0	1.6
30	114	110	114	114	113.0	2.0
31	108	106	112	110	109.0	2.6
32	104	100	106	106	104.0	2.8
33	100	96	100	100	99.0	2.0
34	96	92	96	96	95.0	2.0
35	92	88	92	92	91.0	2.0
36	86	84	86	88	86.0	1.6
37	82	80	82	84	82.0	1.6
38	78	76	78	80	78.0	1.6
39	74	72	74	76	74.0	1.6
40	72	68	70	72	70.5	1.9
41	66	64	66	68	66.0	1.6
42	62	60	62	64	62.0	1.6
43	58	56	58	60	58.0	1.6
44	54	52	54	56	54.0	1.6
45	52	50	50	54	51.5	1.9
46	46	46	46	48	46.5	1.0

Table A6. Configuration F mass data.

Time (min)	Run 1 Mass (g)	Run 2 Mass (g)	Run 3 Mass (g)	Run 4 Mass (g)	Average Mass (g)	SD (g)
0	300	300	300	300	300.0	0.0
1	295	294	295	295	294.8	0.5
2	289	289	289	290	289.3	0.5
3	285	284	284	284	284.3	0.5
4	279	279	279	279	279.0	0.0
5	274	275	273	274	274.0	0.8
6	269	269	269	269	269.0	0.0
7	264	265	263	263	263.8	1.0
8	259	260	258	258	258.8	1.0
9	254	255	253	253	253.8	1.0
10	250	250	249	248	249.3	1.0
11	245	246	244	243	244.5	1.3
12	240	241	240	239	240.0	0.8
13	235	236	235	234	235.0	0.8
14	231	232	230	229	230.5	1.3
15	226	228	226	224	226.0	1.6
16	222	223	221	220	221.5	1.3
17	217	219	217	215	217.0	1.6
18	212	215	213	211	212.8	1.7
19	208	210	208	207	208.3	1.3
20	204	206	204	202	204.0	1.6
21	200	202	200	198	200.0	1.6
22	195	198	196	194	195.8	1.7
23	191	193	192	190	191.5	1.3
24	187	189	188	186	187.5	1.3
25	183	185	183	182	183.3	1.3
26	179	181	180	178	179.5	1.3
27	175	178	176	175	176.0	1.4
28	171	174	172	171	172.0	1.4
29	167	170	168	167	168.0	1.4
30	163	166	164	164	164.3	1.3
31	160	162	161	160	160.8	1.0
32	156	159	157	156	157.0	1.4
33	152	155	153	153	153.3	1.3
34	149	151	150	149	149.8	1.0
35	146	148	146	146	146.5	1.0
36	142	145	143	142	143.0	1.4
37	138	141	139	139	139.3	1.3
38	135	138	136	135	136.0	1.4
39	132	134	132	132	132.5	1.0
40	128	131	129	129	129.3	1.3
41	125	128	126	126	126.3	1.3
42	122	125	123	123	123.3	1.3
43	119	121	120	119	119.8	1.0
44	115	118	117	116	116.5	1.3
45	112	115	113	113	113.3	1.3
46	109	112	110	110	110.3	1.3
47	106	108	107	107	107.0	0.8
48	103	105	104	104	104.0	0.8
49	100	103	101	101	101.3	1.3
50	97	100	98	98	98.3	1.3
51	94	97	95	95	95.3	1.3
52	91	94	92	93	92.5	1.3
53	89	91	89	90	89.8	1.0
54	86	88	86	87	86.8	1.0
55	83	85	84	84	84.0	0.8
56	80	83	81	81	81.3	1.3

Table A6. *Cont.*

Time (min)	Run 1 Mass (g)	Run 2 Mass (g)	Run 3 Mass (g)	Run 4 Mass (g)	Average Mass (g)	SD (g)
57	77	80	78	79	78.5	1.3
58	75	77	75	76	75.8	1.0
59	72	74	72	73	72.8	1.0
60	69	72	70	71	70.5	1.3
61	67	69	67	69	68.0	1.2
62	65	66	64	66	65.3	1.0
63	62	64	62	64	63.0	1.2
64	59	61	59	61	60.0	1.2
65	57	59	57	59	58.0	1.2
66	54	56	54	57	55.3	1.5
67	52	54	52	54	53.0	1.2
68	50	51	49	52	50.5	1.3
69	47	49	47	49	48.0	1.2

References

1. Padmanaban, S.; Nithiyananthan, K.; Karthikeyan, S.P.; Holm-Nielsen, J.B. *Microgrids*, 1st ed.; CRC Press: Boca Raton, FL, USA, 2020; ISBN 978-0-367-81592-9.
2. Raya-Armenta, J.M.; Bazmohammadi, N.; Avina-Cervantes, J.G.; Sáez, D.; Vasquez, J.C.; Guerrero, J.M. Energy Management System Optimization in Islanded Microgrids: An Overview and Future Trends. *Renew. Sustain. Energy Rev.* **2021**, *149*, 111327. [CrossRef]
3. Haerer, R. Whack-a-Mole Fuel Selection: Reducing Operational Risks and Mitigating New Challenges in the US Department of Defense. Climate and Security Fellowship Program, 2021. Available online: https://climateandsecurity.org/wp-content/uploads/2021/10/Climate-Security-Risk-Briefers_Climate-and-Security-Fellows-Program_October-2021-1.pdf#page=27 (accessed on 6 November 2022).
4. Ton, D.T.; Smith, M.A. The U.S. Department of Energy's Microgrid Initiative. *Electr. J.* **2012**, *25*, 84–94. [CrossRef]
5. Holdmann, G.P.; Wies, R.W.; Vandermeer, J.B. Renewable Energy Integration in Alaska's Remote Islanded Microgrids: Economic Drivers, Technical Strategies, Technological Niche Development, and Policy Implications. *Proc. IEEE* **2019**, *107*, 1820–1837. [CrossRef]
6. Van Broekhoven, S.; Judson, N.; Galvin, J.; Marqusee, J. Leading the Charge: Microgrids for Domestic Military Installations. *IEEE Power Energy Mag.* **2013**, *11*, 40–45. [CrossRef]
7. Kafetzis, A.; Ziogou, C.; Panopoulos, K.D.; Papadopoulou, S.; Seferlis, P.; Voutetakis, S. Energy Management Strategies Based on Hybrid Automata for Islanded Microgrids with Renewable Sources, Batteries and Hydrogen. *Renew. Sustain. Energy Rev.* **2020**, *134*, 110118. [CrossRef]
8. Ganesan, S.; Subramaniam, U.; Ghodke, A.A.; Elavarasan, R.M.; Raju, K.; Bhaskar, M.S. Investigation on Sizing of Voltage Source for a Battery Energy Storage System in Microgrid With Renewable Energy Sources. *IEEE Access* **2020**, *8*, 188861–188874. [CrossRef]
9. Liu, J.; Chen, H.; Zhang, W.; Yurkovich, B.; Rizzoni, G. Energy Management Problems Under Uncertainties for Grid-Connected Microgrids: A Chance Constrained Programming Approach. *IEEE Trans. Smart Grid* **2017**, *8*, 2585–2596. [CrossRef]
10. Ismail, M.S.; Moghavvemi, M.; Mahlia, T.M.I.; Muttaqi, K.M.; Moghavvemi, S. Effective Utilization of Excess Energy in Standalone Hybrid Renewable Energy Systems for Improving Comfort Ability and Reducing Cost of Energy: A Review and Analysis. *Renew. Sustain. Energy Rev.* **2015**, *42*, 726–734. [CrossRef]
11. Altin, M.; Hansen, A.D.; Barlas, T.K.; Das, K.; Sakamuri, J.N. Optimization of Short-Term Overproduction Response of Variable Speed Wind Turbines. *IEEE Trans. Sustain. Energy* **2018**, *9*, 1732–1739. [CrossRef]
12. Rahman, M.M.; Oni, A.O.; Gemechu, E.; Kumar, A. Assessment of Energy Storage Technologies: A Review. *Energy Convers. Manag.* **2020**, *223*, 113295. [CrossRef]
13. Koohi-Fayegh, S.; Rosen, M.A. A Review of Energy Storage Types, Applications and Recent Developments. *J. Energy Storage* **2020**, *27*, 101047. [CrossRef]
14. Musolino, V.; Pievatolo, A.; Tironi, E. A Statistical Approach to Electrical Storage Sizing with Application to the Recovery of Braking Energy. *Energy* **2011**, *36*, 6697–6704. [CrossRef]
15. O'Callaghan, O.; Donnellan, P. Liquid Air Energy Storage Systems: A Review. *Renew. Sustain. Energy Rev.* **2021**, *146*, 111113. [CrossRef]
16. Damak, C.; Leducq, D.; Hoang, H.M.; Negro, D.; Delahaye, A. Liquid Air Energy Storage (LAES) as a Large-Scale Storage Technology for Renewable Energy Integration—A Review of Investigation Studies and near Perspectives of LAES. *Int. J. Refrig.* **2020**, *110*, 208–218. [CrossRef]
17. Borri, E.; Tafone, A.; Romagnoli, A.; Comodi, G. A Review on Liquid Air Energy Storage: History, State of the Art and Recent Developments. *Renew. Sustain. Energy Rev.* **2021**, *137*, 110572. [CrossRef]

18. Wang, S.X.; Xue, X.D.; Zhang, X.L.; Guo, J.; Zhou, Y.; Wang, J.J. The Application of Cryogens in Liquid Fluid Energy Storage Systems. *Phys. Procedia* **2015**, *67*, 728–732. [CrossRef]
19. Benato, A.; Stoppato, A. Pumped Thermal Electricity Storage: A Technology Overview. *Therm. Sci. Eng. Prog.* **2018**, *6*, 301–315. [CrossRef]
20. Joshi, D.M.; Patel, H.K. Analysis of Cryogenic Cycle with Process Modeling Tool: Aspen HYSYS. *J. Instrum.* **2015**, *10*, T10001. [CrossRef]
21. Howe, T.A.; Pollman, A.G.; Gannon, A.J. Operating Range for a Combined, Building-Scale Liquid Air Energy Storage and Expansion System: Energy and Exergy Analysis. *Entropy* **2018**, *20*, 770. [CrossRef]
22. Willis, R.; Pollman, A.; Gannon, A.; Hernandez, A. Preliminary Modeling of a Building-Scale Liquid Air Energy Storage Systems Using Aspen HYSYS. In Proceedings of the 2018 MORS Symposium, Monterey, CA, USA, 18–21 June 2018.
23. Girouard, C.; Pollman, A.; Hernandez, A. Modeling and Simulation Informed Conceptual Design, Analysis, and Initial Component Selection of A Supply-Side Building Scale Laes System for Renewable, Islanded Microgrid Resiliency. In Proceedings of the 87th Military Operations Society Symposium, Colorado Springs, CO, USA, 17–20 June 2019.
24. Fredrickson, A.; Pollman, A.; Gannon, A.; Smith, W. Selection of a Heat Exchanger for a Small-Scale Liquid Air Energy Storage System. In Proceedings of the ASME 2021 Power Conference, Anaheim, CA, USA, 20–22 July 2021.
25. Swanson, H.M.; Pollman, A.G.; Hernandez, A. Experimental Evaluation of Dewar Volume and Cryocooler Cold Finger Size in a Small-Scale Stirling Liquid Air Energy Storage (LAES) System. In Proceedings of the ASME 2021 Power Conference, Virtual, 20–22 July 2021.
26. Torosyan, M.; Pollman, A.; Gannon, A.; Hernandez, A. Performance and Complexity Trade Study of Candidate Liquid Air Generation Techniques. In Proceedings of the ASME 2021 Power Conference, Virtual, 20–22 July 2021.
27. Bailey, N.A.; Girouard, C.M.; Pollman, A.G. Dual Stirling Cycle Liquid Air Battery. U. S. Patent 20220042478A1, 10 February 2022.
28. Arnold, S.; Fackrell, C.; Horton, D.; Pollman, A.; Smeeks, F.; Sweet, J. Need, Function, and Requirements Analysis for Liquid Air Energy Storage Prototype on a Military Microgrid. In Proceedings of the MORS Symposium, Quantico, VA, USA, 13–16 June 2022.
29. Lobunets, Y. Thermoelectric Generator for Utilizing Cold Energy of Cryogen Liquids. *J. Electron. Mater.* **2019**, *48*, 5491–5496. [CrossRef]
30. Barron, R.; Nellis, G. *Cryogenic Heat Transfer*, 2nd ed.; CRC Press: Boca Raton, FL, USA, 2016; ISBN 978-1-4822-2744-4.
31. Bostock, T.D.; Scurlock, R.G. *Low-Loss Storage and Handling of Cryogenic Liquids: The Application of Cryogenic Fluid Dynamics*; Springer: Berlin, Germany, 2019; ISBN 978-3-030-10641-6.
32. Lynam, P.; Mustafa, A.; Proctor, W.; Scurlock, R. Reduction of the Heat Flux into Liquid Helium in Wide Necked Metal Dewars. *Cryogenics* **1969**, *9*, 242–247. [CrossRef]
33. Swartz, E.T. Efficient Cryogenic Design, a System Approach. *J. Low Temp. Phys.* **1995**, *101*, 249–252. [CrossRef]
34. Bailey, N.A.; Pollman, A.G.; Paulo, E.P. Energy Recovery for Dual-Stirling Liquid Air Energy Storage Prototype. In Proceedings of the ASME 2020 Power Conference collocated with the 2020 International Conference on Nuclear Engineering, Virtual, 4–5 August 2020.
35. National Institute of Standards and Technology. Available online: https://www.nist.gov/ (accessed on 16 August 2022).